



# The influence of impurity ions on the permeation and oxygen reduction properties of $\text{Ba}_{0.5}\text{Sr}_{0.5}\text{Co}_{0.8}\text{Fe}_{0.2}\text{O}_{3-\delta}$ perovskite

Yubo Chen<sup>a</sup>, Baoming Qian<sup>a</sup>, Sidian Li<sup>b</sup>, Yong Jiao<sup>b</sup>, Moses O. Tade<sup>d</sup>, Zongping Shao<sup>c,d,\*</sup>

<sup>a</sup> State Key Laboratory of Materials-Oriented Chemical Engineering, College of Chemistry & Chemical Engineering, Nanjing University of Technology, No. 5 Xin Mofan Road, Nanjing 210009, PR China

<sup>b</sup> Institute of Molecular Science, Shanxi University, Taiyuan 030006, PR China

<sup>c</sup> College of Energy, Nanjing University of Technology, No. 5 Xin Mofan Road, Nanjing 210009, PR China

<sup>d</sup> Department of Chemical Engineering, Curtin University, Perth, WA 6845, Australia

## ARTICLE INFO

### Article history:

Received 26 June 2013

Received in revised form

9 August 2013

Accepted 13 August 2013

Available online 30 August 2013

### Keywords:

Electrical conductivity

Sintering

Oxygen permeation membrane

Solid oxide fuel cells

Oxygen reduction

## ABSTRACT

This study aims to exploit the effects of little impurity ions on the properties and performance of  $\text{Ba}_{0.5}\text{Sr}_{0.5}\text{Co}_{0.8}\text{Fe}_{0.2}\text{O}_{3-\delta}$  (BSCF) towards the development of membranes for oxygen separation and electrodes for oxygen reduction. The influences of impurity ions ( $\text{Na}^+$ ,  $\text{K}^+$ ,  $\text{Mg}^{2+}$ ,  $\text{Ca}^{2+}$ ,  $\text{Cr}^{x+}$ ,  $\text{Mn}^{x+}$ ,  $\text{Si}^{4+}$  and  $\text{Cl}^-$ ) on the crystal structure, electrical conductivity, oxygen desorption/permeation behavior, sintering behavior and oxygen reduction activity of BSCF were systematically investigated. Rietveld refinements of the powder X-ray diffraction patterns revealed that most of the impurity ions, except  $\text{Mg}^{2+}$  and  $\text{Si}^{4+}$ , can incorporate into the BSCF lattice without changing the lattice symmetry or forming new phases. The membrane containing the  $\text{Mg}^{2+}$  impurity exhibited a reduced grain size, whereas the membrane containing the  $\text{Cl}^-$  impurity exhibits poor sintering ability. The fluctuation in the oxygen permeation flux of the BSCF membranes could be correlated to their different sintering abilities and to the site doped with the impurity ions. The impedance spectra of symmetrical cells with BSCF electrodes containing various impurity ions showed that the small impurity ions did not strongly affect the electrode performance. These results suggested that low purity raw materials could be used to prepare BSCF materials, thus improving their economic attractiveness.

© 2013 Elsevier B.V. All rights reserved.

## 1. Introduction

Perovskite oxides are one class of important functional materials that have a wide range of potential applications; these oxides have the general formula  $\text{ABO}_3$  and are generally built up with a framework of vertex-sharing  $\text{BO}_6$  octahedra with the large A-site cation located in a position with 12-fold coordination. Due to the high flexibility of the cations in both the A and B sites, a wide range of properties that are important for various applications could be achieved through doping. Within the perovskite oxide family, the oxides possessing mixed ionic and electronic conductivity are of special importance and have been exploited as materials for ceramic membranes (CMs) for oxygen separation, electrodes for solid oxide fuel cells (SOFCs) for efficient power generation and solid oxide electrolysis cells (SOECs) for hydrogen generation.

\* Corresponding author at: College of Energy, Nanjing University of Technology, No. 5 Xin Mofan Road, Nanjing 210009, PR China. Tel.: +86 25 83172256; fax: +86 25 83172242.

E-mail address: [shaozp@njut.edu.cn](mailto:shaozp@njut.edu.cn) (Z. Shao).

Many mixed conducting perovskite oxides, such as  $\text{La}_{0.6}\text{Sr}_{0.4}\text{Co}_{0.2}\text{Fe}_{0.8}\text{O}_{3-\delta}$  (LSCF),  $\text{Sm}_{0.5}\text{Sr}_{0.5}\text{CoO}_{3-\delta}$  (SSC) and  $\text{Ba}_{0.5}\text{Sr}_{0.5}\text{Co}_{0.8}\text{Fe}_{0.2}\text{O}_{3-\delta}$  (BSCF), that show high surface activity and bulk oxygen mobility at elevated temperatures have been developed [1–3]. The properties of perovskite oxides, such as their crystal structure, structural stability, surface activity, bulk ionic/electronic conductivity, sintering behavior, thermal expansion and mechanical strength, are all closely related to the cations and anions in their lattice structure. Recently, ionic modifications, such as cation/anion doping in both the A and B sites and introducing deliberate deficiencies in the A/B sites, have been widely applied to improve the properties of perovskite oxides and consequently their performance in the above-mentioned application fields. For example,  $\text{BaFeO}_{3-\delta}$  shows several crystal structures at different temperatures; the oxygen-disordered cubic structure is only stable at elevated temperatures, whereas the room temperature crystal structure is highly dependent on the oxygen content in the oxide lattice. However, the cubic Pm-3m phase is successfully stabilized at room temperature for  $\text{Ba}_{0.95}\text{La}_{0.05}\text{FeO}_{3-\delta}$ , which was obtained by simply substituting only 5%  $\text{Ba}^{2+}$  in the A-site of  $\text{BaFeO}_3$  with  $\text{La}^{3+}$ , making it a suitable material for CMs and for the cathodes of SOFCs [4,5]. The performance of conducting perovskite oxides can also be improved by introducing cation vacancies in their structures.

For example, Liu et al. observed that the electrode polarization resistance of SOFCs using an A-site cation deficient  $\text{Ba}_{1-x}\text{Co}_{0.7}\text{Fe}_{0.2}\text{Nb}_{0.1}\text{O}_{3-\delta}$  was greatly reduced compared to the stoichiometric  $\text{Ba}_1\text{Co}_{0.7}\text{Fe}_{0.2}\text{Nb}_{0.1}\text{O}_{3-\delta}$ ; furthermore, the detrimental phase reaction between  $\text{Ba}_{1-x}\text{Co}_{0.7}\text{Fe}_{0.2}\text{Nb}_{0.1}\text{O}_{3-\delta}$  and the gadolinia doped ceria electrolyte layer was mediated [6].

Among the various mixed conducting perovskite oxides, BSCF exhibits extraordinary high oxygen ion transport properties and has recently received considerable research attention for use in CMs and as an oxygen reduction electrode (cathode) for SOFCs [7]. In 2000, Shao et al. first developed and applied BSCF as the material for CMs for oxygen separation, and a high oxygen permeation flux of  $\sim 1.6 \text{ mL cm}^{-2} \text{ min}^{-1}$  [STP] at  $900^\circ\text{C}$  with a membrane thickness of 1.5 mm was achieved [8]. Later, Shao et al. also demonstrated that BSCF possessed considerable electrochemical activity for oxygen reduction at intermediate temperatures [9]. Following these reports, a considerable number of studies have been conducted to further improve the properties and performance of BSCF, such as through doping its A-site ( $\text{Ba}^{2+}/\text{Sr}^{2+}$ ) and/or B-site ( $\text{Co}^{3+}/\text{Fe}^{3+}$ ) with  $\text{Sm}^{3+}$ ,  $\text{Cr}^{4+}$ ,  $\text{Mn}^{4+}$ ,  $\text{Zr}^{4+}$ ,  $\text{Ti}^{4+}$ , or  $\text{Nb}^{5+}$  [10–13]. For example, Lu et al. reported that the substitution of some transition metals ( $\text{Cr}^{3+}$ ,  $\text{Mn}^{4+}$ , and  $\text{Zr}^{4+}$ ) for  $\text{Fe}^{3+}$  clearly affected the crystal structure, structural stability and oxygen permeability of the BSCF membrane, whereas substituting  $\text{Sm}^{3+}$  for Ba/Sr in the A-site resulted in increased electrical conductivity. Furthermore, A- or B-site cation deficiencies were also found to have a clear effect on the properties and performance of BSCF for use as CMs and as an oxygen reduction electrode [14–17].

To date, the majority of dopants that have been used in doping BSCF have substituted at least 5 mol% of the A- or B-site cations [10–13,18,19]. It is well known that the raw materials used in the synthesis of powders unavoidably contain a certain level of impurities. The concentration of such impurities, depending on the grade of the raw material, may reach as high as 1%. Low purity raw materials are less expensive, which makes them attractive for commercial use. However, after synthesis, such impurities may be doped into the perovskite lattice or remain as an impurity phase at the grain boundaries of the perovskite oxide, which could affect the properties, such as conductivity and sintering, and subsequently the performance of BSCF for functional applications. In fact, it is well established in the literature that the presence of trace amounts of dopants can greatly alter the magnetic and electrical properties of some perovskite oxides [20–22]. In addition, many studies have investigated and proved the impurity elements, such as sulfur, silicon and chromium, from the surrounding gas atmosphere have a great influence on the performance of CMs and SOFCs [23–25]. However, until now, the effects of minor amounts of impurities originating from raw materials on the properties and performances of mixed conducting oxides have rarely been reported in the literature. If the impurity has a negligible influence on the properties and performance of perovskite for use in CMs or SOFCs, an effective reduction in cost could be realized by using lower purity raw materials.

In the present work, some elements that could easily be treated as impurities in raw materials, including Na, K, Mg, Ca, Cr, Mn, Si and Cl, were added deliberately during the preparation of BSCF, and the concentration of these elements was fixed at 1 mol% of the total cations in BSCF and such mole ratio is a relative high amount for impurities. The properties, such as the crystal structure, oxygen desorption behavior, electrical conductivity, sintering behavior, performance as a ceramic membrane for oxygen separation and activity as an electrode for oxygen reduction, were systematically investigated. The purpose of this study is to clarify whether it is necessary to use high purity raw materials during the synthesis of BSCF for applications as an oxygen separation membrane and as an oxygen reduction electrode.

## 2. Experimental

### 2.1. Sample fabrication

A series of BSCF-M (M=Na, K, Mg, Ca, Cr, Mn, Si, and Cl) powders were prepared by the EDTA-citrate complexing method [26]. The pristine BSCF powder was synthesized for comparison. During the synthetic process, 1 mol% of the metal nitrates of the desired impurities (ethyl-silicate and  $\text{Mn}(\text{CH}_3\text{COO})_2 \cdot 4\text{H}_2\text{O}$  were applied as the source materials for Si and Mn, respectively) were introduced. To introduce the Cl impurity, a partial amount of Co ( $\text{NO}_3$ )<sub>2</sub> was replaced by  $\text{CoCl}_2 \cdot 6\text{H}_2\text{O}$  during the synthesis of BSCF. The target powder was obtained by calcining the precursor at  $950^\circ\text{C}$  for 5 h.

The bars used for the electrical conductivity tests and the membranes (diameter of 15 mm) used for the oxygen permeation tests were prepared via the dry pressing method with a stainless steel die. After pressing, the bars and membranes were sintered at  $1100^\circ\text{C}$  for 5 h to ensure a high density.

### 2.2. Characterization and analysis

For X-ray diffraction (XRD) characterization, all powders were first ground by hand with an agate mortar to obtain homogeneous particles. The XRD data of the samples were recorded using a Rigaku Smartlab X-ray diffraction system under the following conditions: 40 kV, 200 mA, Cu K $\alpha$  radiation, and at room temperature. The samples were continuously scanned over the range from  $20^\circ$  to  $90^\circ$  ( $2\theta$ ) using a step size of  $0.02^\circ$  ( $2\theta$ ). The General Structure Analysis System (GSAS) with the EXPGUI interface was applied for the Rietveld refinement of the XRD data [27]. During the refinement, the Thompson–Cox–Hastings function and a 12-term shifted Chebyshev polynomial function were applied to refine the peak shape and background, respectively [28]. The isotropic atomic displacement parameters ( $U_{\text{iso}}$ ) were refined, and the  $U_{\text{iso}}$  of the atoms at the same position were constrained to be equal. The occupancy parameter of the oxygen atom was constrained to be equal to one due to the limitations of X-ray scattering by light atoms in the presence of barium and strontium.

The electrical conductivity was measured using the D.C. four-point probe method over a temperature range of  $300$ – $900^\circ\text{C}$  in ambient air at a cooling rate of  $5^\circ\text{C min}^{-1}$ , and a digital Sourceter (Keithley 2420, USA) using a four-probe configuration was applied to the test. Silver leads were attached to the bar ( $\sim 10 \text{ mm} \times 5 \text{ mm} \times 2 \text{ mm}$ ) with the help of silver paste (DAD-87, Shanghai Research Institute of Synthetic Resins) to form the current and potential probes.

The effects of impurities on the oxygen desorption properties of BSCF were studied using the oxygen-temperature-programmed desorption ( $\text{O}_2$ -TPD) technique. The sample powder was first pressed into a membrane, which was then crushed to produce particles for the  $\text{O}_2$ -TPD test. Approximately 0.15 g of particles was loaded into a U-type quartz tube. Helium was used as carrier gas at a flow rate of  $15 \text{ mL min}^{-1}$ , and the sample was heated to  $930^\circ\text{C}$  at a rate of  $10^\circ\text{C min}^{-1}$ . The released oxygen was detected using an online mass spectrometer (QIC-20, Hiden). The sintering behaviors of the samples were further studied with SEM (TM3000, Hitachi), and the oxygen permeation test was performed with a gas chromatograph (CP-3800, Varian). Helium was used as the sweeping gas at a flow rate of  $30 \text{ mL min}^{-1}$  and ambient air was applied as the feed gas.

The oxygen permeation flux was calculated using the following equation:

$$J_{\text{O}_2} (\text{mL min}^{-1} \text{ cm}^{-2}) = (C_{\text{O}_2} - C_{\text{N}_2} \times 0.21/0.79 \times \sqrt{28/32}) \times F/S$$

where  $C_{\text{O}_2}$  and  $C_{\text{N}_2}$  are the measured concentrations of oxygen and nitrogen in the sweeping gas, respectively.  $F$  is the flow rate of the

sweeping gas.  $S$  is the effective area of the membrane on the sweeping side.

Based on the configuration of the symmetrical cell, the oxygen reduction activities of the samples were measured using an electrochemistry work station (Solartron 1260+Solartron 1287). The samples were deposited on both sides of SDC electrolyte pellets with an area of  $\sim 0.6 \text{ cm}^2$ , and the symmetrical cells were sintered at  $1000 \text{ }^\circ\text{C}$  for 2 h in air. Diluted silver paste was used as the current collector. Frequencies ranging from 0.01 to  $10^5 \text{ Hz}$  were applied, and the signal amplitude was 10 mV.

### 3. Results and discussion

#### 3.1. Properties

##### 3.1.1. Crystal structure

The effects of a small amount (1 mol% of the total cations in BSCF) of the various impurity ions on the crystal structure of BSCF were first studied using room temperature powder XRD. For use as an electrode for SOFCs, BSCF is usually synthesized at approximately  $950 \text{ }^\circ\text{C}$ . Thus, the phase composition of the samples containing the various impurity ions calcined at  $950 \text{ }^\circ\text{C}$  for 5 h was analyzed first. Due to the high intensity of the X-ray beam, not all of the radiation with  $K_{\beta} = 1.39225 \text{ \AA}$  was effectively filtered; thus, peaks in very weak intensity representing the (110), (200) and (211) plane of BSCF at approximately  $28.8^\circ$ ,  $41^\circ$  and  $50.6^\circ$  ( $2\theta$ ) can be observed in some XRD patterns. As shown in Fig. 1, for all samples, the main diffraction peaks were well indexed based on a basic BSCF cubic perovskite structure. However, additional peaks with weak intensities that correspond to impurity phases were observed; most of these peaks were assigned to  $(\text{Ba,Sr})\text{CoO}_3$ ,  $(\text{Ba,Sr})\text{CO}_3$  and CoO. To determine if the impurity phases are thermodynamically stable, the various samples were further treated at  $1000 \text{ }^\circ\text{C}$  for 2 h or  $1100 \text{ }^\circ\text{C}$  for 5 h. The former is the normal calcination condition used to prepare the BSCF electrode for a SOFC, whereas the latter is the preparation condition applied to prepare CMs using the BSCF material. For simplicity, the samples that were further calcined at  $1000 \text{ }^\circ\text{C}$  and  $1100 \text{ }^\circ\text{C}$  were named BSCF-M1000 and BSCF-M1100 ( $M = \text{Na, K, Mg, Ca, Cr, Mn, Si, and Cl}$ ), respectively. The XRD patterns of the various samples after the additional calcinations at  $1000 \text{ }^\circ\text{C}$  and  $1100 \text{ }^\circ\text{C}$  are shown in Fig. 2. Impurity peaks corresponding to  $(\text{Ba, Sr})\text{CoO}_3$  and CoO can still be observed in the sample containing the  $\text{Mg}^{2+}$  impurity after the additional calcination at  $1000 \text{ }^\circ\text{C}$ ; however, only CoO remained in the sample that was calcined at the higher temperature ( $1100 \text{ }^\circ\text{C}$ ). For the other samples, all of the diffraction peaks can be indexed based on the BSCF perovskite structure. This result suggests that although some impurity ions could still remain as separate phases when the synthesis temperature was  $950 \text{ }^\circ\text{C}$ , the majority of these impurity ions were

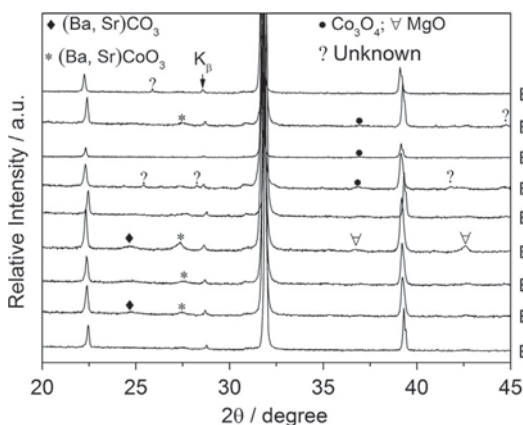


Fig. 1. XRD patterns of all samples sintered at  $950 \text{ }^\circ\text{C}$  for 5 h.

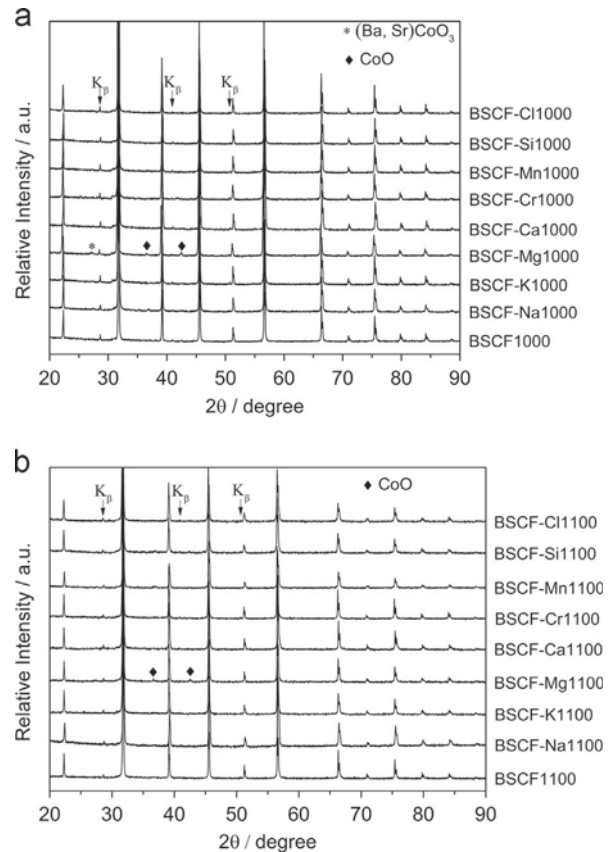


Fig. 2. XRD patterns of samples with additional heat treatments at  $1000 \text{ }^\circ\text{C}$  for 2 h (a) and  $1100 \text{ }^\circ\text{C}$  for 5 h (b).

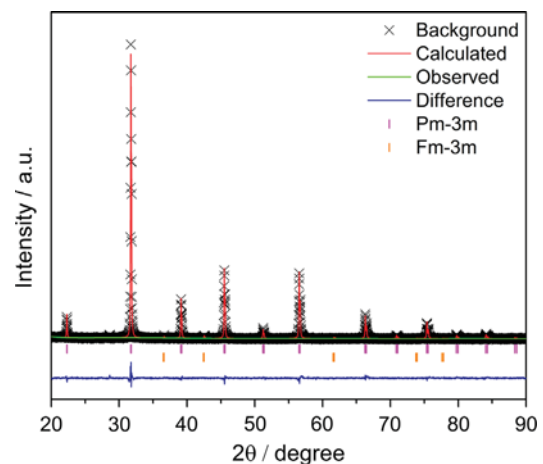


Fig. 3. Rietveld refinement for BSCF-Mg1100, in which CoO (Fm-3m) is considered as the second phase.

successfully incorporated into the BSCF lattice by increasing the firing temperature to  $1000 \text{ }^\circ\text{C}$  or higher. For each sample calcined at  $1100 \text{ }^\circ\text{C}$ , a shift of the diffraction peaks towards lower angles was observed compared to that of the sample calcined at  $1000 \text{ }^\circ\text{C}$ . That is, the crystal lattice of the samples expanded after calcination at the higher temperature. This result can be explained by the thermal reduction of the cobalt and iron ions in the BSCF lattice, which resulted in the B-site cations having an increased average ionic radius.

To obtain further information about the influence of these impurity ions on the BSCF crystal structure, Rietveld refinement was specifically conducted to analyze the samples after calcining at  $1100 \text{ }^\circ\text{C}$ . During the refinement, initial structure information from

**Table 1**  
Refined lattice parameters and reliability factors.

Sample	BSCF1100	BSCF–Na1100	BSCF–K1100	BSCF–Mg1100 <sup>a</sup>	BSCF–Ca1100	BSCF–Cr1100	BSCF–Mn1100	BSCF–Si1100	BSCF–Cl1100
Lattice parameter (Å)	3.984(0)	3.983(7)	3.985(8)	3.985(5)	3.981(5)	3.988(6)	3.985(6)	3.983(7)	3.982(9)
$\chi^2$	1.713	1.622	1.357	1.485	2.436	1.890	1.458	1.467	1.744
R <sub>p</sub> (%)	3.74	3.92	3.43	3.51	4.03	4.04	3.96	3.39	3.67
R <sub>wp</sub> (%)	4.92	2.93	4.37	4.53	5.68	5.24	5.07	4.32	4.85

<sup>a</sup> The lattice parameter of the CoO phase in BSCF–Mg1100 is not listed here.

ICSD #109642 and #245319 was adopted for BSCF and CoO, respectively. The XRD patterns of BSCF1100, BSCF–Na1100, BSCF–K1100, BSCF–Ca1100, BSCF–Cr1100, BSCF–Mn1100, BSCF–Si1100 and BSCF–Cl1100 were all successfully refined using the Pm-3 m space group. When refining the structure of BSCF–Mg1100, CoO with the Fm-3 m space group was added as the second phase, as shown in Fig. 3. The refined lattice parameters and reliability factors are listed in Table 1. As shown, reliable discrepancy factors were obtained for all of these samples. An expansion of the BSCF lattice was observed with the presence of the K, Mg, Cr and Mn impurity elements, whereas contraction of the BSCF lattice was observed with the presence of Na, Ca, Cl and Si as the impurity elements.

There are several possibilities for the presence of impurity ions in the BSCF system after calcination at elevated temperatures. In one case, these impurity ions failed to incorporate into the BSCF perovskite lattice; instead, they were present as separate phase(s) (amorphous or crystalline). It is well known that many elements can be doped into the perovskite structure, and more than 90% of all elements have been reported to be successfully doped into the perovskite lattice. All of the impurity ions investigated in this study have previously been found in some perovskite-type oxides in the literature [11,20,29–33]. Generally, there are two cases for a cation to be doped into the perovskite lattice. In one case, impurity ion fully doped into the A/B-site or both the A- and B-sites, in the other case, the impurity ion would exchange with A/B-site cations or both the A- and B-site cations. The exact site that a cation dopes is closely related to its ionic radius, which should match the ionic size of the cations in the site where it is doped. Because once the ionic radius of an impurity ion, lied in the A/B site, is greatly different from the original ionic radius in the A/B site, then a cation ordering and/or structure collapse would occur. So, if the cubic structure of BSCF sustained, the alkaline or alkaline earth ions with large ionic radii, such as Na<sup>+</sup>, K<sup>+</sup>, Ba<sup>2+</sup>, Sr<sup>2+</sup> and Ca<sup>2+</sup>, can only dope into the A-site of the perovskite lattice, whereas most transition metal ions (e.g. Cr<sup>x+</sup>, Mn<sup>x+</sup>, Co<sup>x+</sup> and Fe<sup>x+</sup>) and alkaline/alkaline earth metal ions with smaller ionic radii, such as Li<sup>+</sup> and Mg<sup>2+</sup>, preferentially enter the B-site of the perovskite lattice. As a result, the phase structure of doped BSCF is a key factor used to prove the doping site of these impurity ions. The impurity ions herein are either large or small, so the case that one impurity ion dopes into A site and B site or exchange with A site and B site ions simultaneously are unlikely.

Because the BSCF in this study was designed to have stoichiometry in the A/B cation site, incorporating impurity ions into the A- or B-site without exchanging cations with the parent oxide (BSCF) should result in a cation deficient BSCF. In contrast, a cation-stoichiometric perovskite can still be obtained if the impurity ions exchange with the cations in BSCF. However, in this case, impurity phase(s) should be formed.

In the A-site of a perovskite oxide, which is in 12-fold coordination with oxygen ions, Ca<sup>2+</sup>, Sr<sup>2+</sup>, Ba<sup>2+</sup>, Na<sup>+</sup> and K<sup>+</sup> cations have ionic radii of 1.31, 1.44, 1.61, 1.39 and 1.71 Å, respectively [34]. These ionic radii suggest that doping Ca<sup>2+</sup> and Na<sup>+</sup> into the A-site of BSCF would result in contraction of the lattice, whereas doping K<sup>+</sup> into the A-site would result in expansion of the lattice; this hypothesis is

consistent with the experimental observation. Because the lattice parameter is determined by both the A- and B-site cations, the reduced lattice parameter implies that the effective ionic size of the B-site cation should also be reduced after incorporating Ca<sup>2+</sup> and Na<sup>+</sup> into the A-site of BSCF, which can be realized by oxidizing the Co/Fe cations in the B-site to a higher oxidation state or by transitioning the B-site cations to a lower spin state. Compared to BSCF–Ca1100, the contraction of the BSCF–Na1100 lattice is not as pronounced, which can be attributed to the large ionic radius of Na<sup>+</sup>. Because no other impurity phase(s) were observed, doping BSCF with Ca<sup>2+</sup>, Na<sup>+</sup> and K<sup>+</sup> should result in the formation of a B-site cation deficiency. We have previously demonstrated that BSCF can indeed tolerate a large A- or B-site cation deficiency, up to 15–20% of the total cations in the A- or B-sites [13,15].

Doping cations into the perovskite B-site has a very complex effect on the lattice parameter because the majority of transition metals can adopt multiple valence states and show different spin states (high, low and intermediate), both of which affect the ionic radius of the cation. The lattice expansion of the sample containing the Cr impurity suggested that Cr was also successfully doped into the BSCF lattice, likely into the B-site. It is well known that the normal oxidation state of Cr in a perovskite structure is mainly +3, whereas previous investigations have demonstrated that cobalt and iron in BSCF mainly adopt a lower mean valence state of +2.7 [35,36]. The ionic radii of Cr<sup>3+</sup>, Co<sup>3+</sup> (LS) and Fe<sup>3+</sup> (LS) are 0.615, 0.545 and 0.55 Å, respectively. Therefore, doping the larger Cr<sup>3+</sup> ion into BSCF caused the mean ionic radii of the B-site cations to increase, which caused the lattice to expand. Furthermore, for Mn, the ionic radii of Mn<sup>4+</sup>, Mn<sup>3+</sup>(LS) and Mn<sup>3+</sup>(HS) are 0.53, 0.58 and 0.645 Å. Therefore, the increased lattice parameter indicated that the valence state of the Mn ion in BSCF should partially be trivalent.

Compared to BSCF1100, the BSCF–Cl1100 lattice was contracted. Dai et al. have systematically studied the impact of doping halogens (F, Cl) into perovskite-type materials (La<sub>1-x</sub>Sr<sub>x</sub>FeO<sub>3-δ</sub>, YBa<sub>2</sub>Cu<sub>3</sub>O<sub>7-δ</sub>) [33,37]. They concluded that the halogen was doped into the oxide lattice by occupying the oxygen vacancy sites instead of replacing part of the lattice O<sup>2-</sup> and that the mean valence state of the B-site ion was increased to maintain charge neutrality. In their experiment, an expansion of the lattice was observed after doping with Cl<sup>-</sup>, which is consistent with Cl<sup>-</sup> (1.81 Å) having a larger ionic radius than O<sup>2-</sup> (1.4 Å). However, in the current study, the BSCF–Cl1100 lattice decreased when doped with Cl<sup>-</sup>. Assuming that the Cl<sup>-</sup> also occupied the oxygen vacancy sites in BSCF–Cl1100, the radius of the B-site ion decreased because the mean valence state of the B-site cations increased. Therefore, it appears that the decreased B-site ionic radius plays a leading role in the lattice parameter of BSCF–Cl1100, likely due to the low Cl<sup>-</sup> content.

For the sample containing the Mg<sup>2+</sup> impurity, even after the calcination at 1100 °C (BSCF–Mg1100), the CoO (~1.7 wt%) impurity phase was still present according to the Rietveld refinement (Fig. 3). The refined lattice parameter of CoO of  $a=b=c=4.25(7)$  Å was close to the value reported in the literature [38], and the lattice parameter of the BSCF-related phase was 3.985(0) Å for

BSCF–Mg1100. The expansion of the lattice confirmed that  $\text{Mg}^{2+}$  with a larger ionic radius (0.72 Å) likely doped into the B-site of BSCF. Thus,  $\text{Mg}^{2+}$  likely replaced some Co from the B-site of BSCF accompanied by the formation of the CoO impurity phase after the high temperature calcination (1100 °C); the remainder of the Mg incorporated into the BSCF lattice.

For the sample with the Si impurity, after calcining at 1100 °C (BSCF–Si1100), the lattice parameter was smaller than that of pure BSCF, suggesting that there should be a phase reaction between BSCF and  $\text{SiO}_2$ . Porras–Vazquez et al. observed that doping Si into BSCF could not form a single phase and that the formation of an impurity phase such as  $\text{Sr}_2\text{CoSi}_2\text{O}_7$  was unavoidable [19]. The reason why the impurity phase(s) was not detected by XRD can be attributed to two factors: one was the trace amount of phase reaction products; the other was that the remaining Si would exist as an amorphous phase [39].

### 3.1.2. Oxygen desorption properties

Both oxygen separation with a ceramic membrane and oxygen reduction with an electrode involve bulk oxygen diffusion and surface exchange in perovskite materials.  $\text{O}_2$ -TPD is a facile technique for characterizing the properties of mixed conducting oxides. With the linear increase of temperature under an inert atmosphere, the cations in the B-site can be thermally reduced to a lower oxidation state, which creates a driving force for the biased movement of oxygen ions from the oxide bulk to the surface, where they are consequently oxidized to molecular oxygen via a series of surface exchange processes.  $\text{O}_2$ -TPD can thus provide some useful information about the cations in the perovskite, such as the concentration of reducible cations, the reduce activities of cations, as well as providing information about the bulk oxygen diffusion and surface exchange properties of the oxides. In some cases, a slight change in composition may significantly affect the reducibility of the B-site cations, the oxygen mobility in the oxide bulk and the surface exchange properties, thus resulting in a large change in the shape of  $\text{O}_2$ -TPD profile.

Fig. 4 shows the  $\text{O}_2$ -TPD profiles of the various BSCF samples containing different impurity ions that were pre-calcined at 1100 °C. Similar to most cobalt-containing mixed conducting perovskite oxides, two types of oxygen are released from these samples during the heating process, which can be observed in the  $\text{O}_2$ -TPD profiles. The oxygen released at low temperatures (300–500 °C), denoted as  $\alpha$ -type oxygen, is correlated with the oxygen adsorbed on the oxygen vacancy sites and/or the reduction of high oxidation state  $\text{Co}^{4+}/\text{Fe}^{4+}$  to  $\text{Co}^{3+}/\text{Fe}^{3+}$ . The intensity and onset temperature of the  $\alpha$ -type oxygen desorption peak was dependent on the nature of both the A- and B-site cations. In contrast, the oxygen released at higher temperatures, denoted  $\beta$ -type oxygen, is associated with the further reduction of the B-site cations, i.e., the reduction of  $\text{Co}^{3+}/\text{Fe}^{3+}$  to  $\text{Co}^{2+}/\text{Fe}^{2+}$ . Because the  $\text{Fe}^{3+}$  in BSCF is stable under the  $\text{O}_2$ -TPD experimental conditions, the lattice oxygen released at high temperature is primary caused by the reduction of  $\text{Co}^{3+}$  to  $\text{Co}^{2+}$ .

Different impurity ions resulted in slightly different intensities and/or shapes of the  $\alpha$ -type or  $\beta$ -type oxygen desorption peak. For example, the intensity of the  $\beta$ -type oxygen desorption peak of BSCF–Ca1100 was considerably weaker than that of BSCF1100. This result implied that the  $\text{Co}^{3+}$  in BSCF–Ca1100 was unlikely to be reduced to  $\text{Co}^{2+}$ . As expected, the intensity of the  $\beta$ -type oxygen desorption peak of BSCF–Na1100 was between that of BSCF1100 and BSCF–Ca1100 due to the weaker impact of  $\text{Na}^+$  in BSCF. In contrast, BSCF–K1100 presented a higher intensity  $\beta$ -type oxygen desorption peak than that of BSCF1100. This difference can be explained by doping the larger  $\text{K}^+$  ion into the perovskite lattice, which caused the lattice to expand and consequently promoted

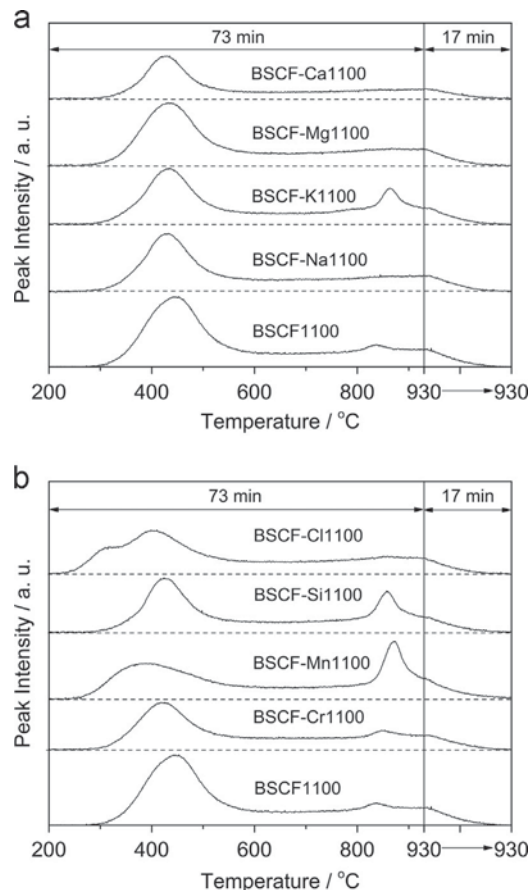


Fig. 4.  $\text{O}_2$ -TPD profiles of samples that were pre-calcined at 1100 °C for 5 h.

the reduction of  $\text{Co}^{3+}$  to  $\text{Co}^{2+}$ . It has been reported that  $(\text{Ba}_{0.5}\text{Sr}_{0.5})_{1.03}\text{Co}_{0.8}\text{Fe}_{0.2}\text{O}_{3-\delta}$  could weaken the Co/Fe–O bond and facilitate oxygen mobility within the oxide lattice [16]. The formation of a B-site cation deficiency as a result of incorporating  $\text{K}^+$  into the A-site of the BSCF lattice may also facilitate the reduction of  $\text{Co}^{3+}$  to  $\text{Co}^{2+}$ . The oxygen desorption behavior of BSCF–Mg1100 was similar to that of pure BSCF1100. This similar desorption behavior can be explained by the fact that the incorporation of  $\text{Mg}^{2+}$  into the BSCF perovskite lattice was realized by the partial replacement of cobalt with  $\text{Mg}^{2+}$  without creating a cation deficiency. Compared to BSCF1100, the onset temperature for the  $\alpha$ -type oxygen desorption peak of BSCF–Cl1100 was reduced, which suggests that doping chlorine into BSCF weakened the A/B–O bond in BSCF to facilitate the dissociation of both  $\alpha$ -type and  $\beta$ -type oxygen.

With respect to the transition metal impurities (Cr, Mn and Si), some different phenomena were observed. For BSCF–Cr1100, a considerably smaller  $\alpha$ -type oxygen desorption peak but a similar  $\beta$ -type oxygen desorption peak compared to those of BSCF1100 were observed, revealing that the enlarged lattice parameter should also be caused by the reduced oxidation state and/or the spin state transition of cobalt and iron. The largest change was observed for the sample containing the  $\text{Mn}^{3+}$  impurity, in which the  $\alpha$ -type oxygen desorption peak became broad and the onset temperature was reduced. More importantly, a distinct  $\beta$ -type oxygen desorption peak appeared at high temperature, indicating that oxygen mobility was facilitated and that  $\text{Co}^{3+}$  was reduced to  $\text{Co}^{2+}$ . The 3d levels of the transition metals in the center of the octahedron split into the  $t_{2g}$  and  $e_g$  sublevels to stabilize the octahedron. The six-fold coordination of  $\text{Mn}^{3+}$  with the  $t_{2g}^3e_g^1$  (d4) electron state does not obey  $O_h$  symmetry and would further split, which may cause octahedral distortion,

i.e., Jahn–Teller distortion. Such a slight local distortion may not be detected by XRD, but it appears to strongly impact the state of the neighboring cobalt.

Abnormal oxygen desorption behavior was observed for the sample containing Si. A distinct and sharp  $\beta$ -type oxygen desorption peak was observed. This observation revealed that the Co/Fe state in BSCF–Si1100 was different from that in pure BSCF and confirmed that a phase reaction between BSCF and Si occurred, as discussed previously. Such an interaction would impact the oxygen reduction behavior of Co/Fe.

### 3.1.3. Electrical conductivity

In addition to high oxygen ion conductivity, sufficient electronic conductivity is also important for a perovskite oxide to be applied as an oxygen permeation membrane or as an oxygen reduction electrode for SOFCs. The electronic conductivity of a perovskite oxide is closely related to the symmetry of the perovskite structure, the spin/valence state of cations, the presence of oxygen vacancies and the presence of impurity phase(s). The D.C. four-point probe method is a facile way to measure the total conductivity of a material. Due to the overwhelming electronic conductivity in BSCF, the measured electrical conductivity mainly reflects the electronic conductivity.

Fig. 5 presents the dependence of the electrical conductivity on temperature for various BSCF oxides containing different impurity ions. Due to the low density and weak mechanical strength of BSCF containing  $\text{Cl}^-$  impurities, the conductivity behavior of  $\text{Cl}^-$  doped BSCF versus temperature cannot be obtained. For pure BSCF, the conductivity measured during cooling is consistent with a previous report [17]. At temperatures lower than  $500^\circ\text{C}$ , the electrical conductivity of BSCF behaves similarly to that of a semiconductor (localized carrier regime) and can be described using the small polaron hopping mechanism presented by Zerner [40]. In situ X-ray absorption and room temperature Mossbauer spectroscopy studies have revealed that the  $\text{Co}^{x+}/\text{Fe}^{x+}$  ions are primarily in the trivalent state with the remainder of these ions in the tetravalent state in the low temperature region; thus, the change in valence state facilitated hole hopping [41,42]. Therefore, as the temperature increased, the holes are activated, which increases the conductivity. As the temperature was further increased ( $> 500^\circ\text{C}$ ), the  $\text{Co}^{4+}/\text{Fe}^{4+}$  were reduced to  $\text{Co}^{3+}/\text{Fe}^{3+}$  and the conductivity remained almost unchanged or slightly decreased (metallic conductivity behavior) with temperature. A semiconducting behavior was observed again at temperatures above  $\sim 700^\circ\text{C}$ , and this phenomenon is attributed to the further reduction of cobalt from  $\text{Co}^{3+}$  to  $\text{Co}^{2+}$ .

The electrical conductivities of all samples are close to each other, but taking the experimental error into consideration, it is unreliable to compare the value of electrical conductivities of each sample, that is which sample possess the highest/lowest electrical conductivity cannot be distinguished. Anyway, the presence of impurity ions did not have a significant influence on the electrical conductivity of BSCF. Roughly, all samples first showed an increase in conductivity followed by a plateau with increasing temperature. This observation is in good agreement with the fact that the main perovskite structure survived for all samples. According to the small-polaron hopping mechanism, the electrical conductivity in this temperature range can be described by the equation:

$$\sigma = (A/T) \exp(-E_a/kT)$$

where  $\sigma$  is the electrical conductivity,  $A$  is a constant parameter,  $T$  is the absolute temperature,  $E_a$  is the activation energy, and  $k$  is the Boltzmann constant. The calculated activation energies of each sample were also very similar, indicating that the impurity ions in BSCF did not affect the conduction mechanism at low temperature. In particular, the conductivity behaviors of various BSCF samples containing  $\text{K}^+$ ,  $\text{Ca}^{2+}$ ,  $\text{Si}^{4+}$  and  $\text{Na}^+$  impurities were similar to that

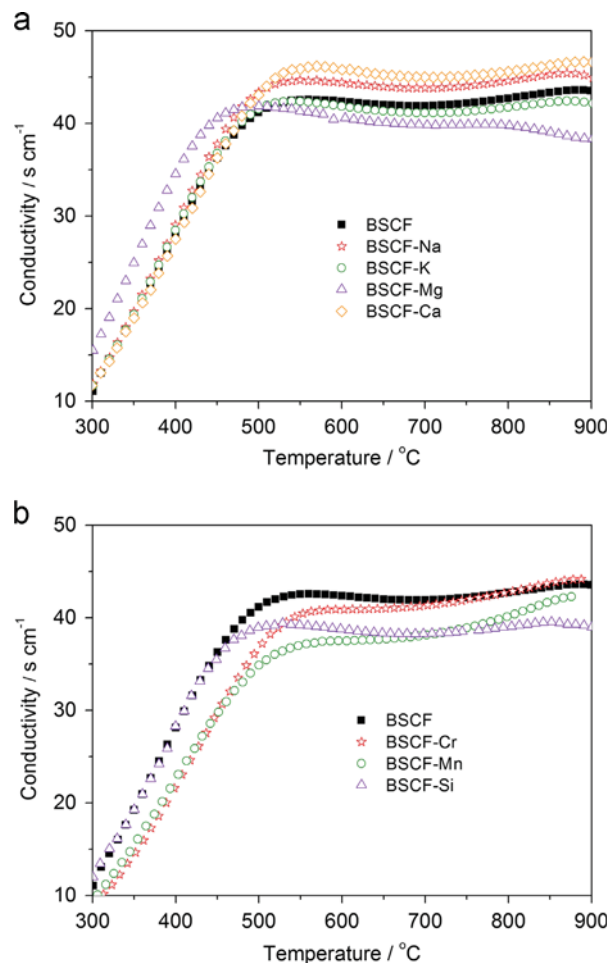


Fig. 5. Electrical conductivities of the various BSCF samples containing different impurities during the cooling process.

of pristine BSCF over the entire temperature range. This result may be because the conductivity behavior of a perovskite is mainly determined by the B-site ions. Especially for the Si-containing BSCF, the conductivity transition of BSCF–Si1100 was similar to that of pure BSCF, suggesting that the presence of impurities and/or a small amount of amorphous silica in BSCF did not cause a significant blocking effect for electrical conductivity around the grain boundary.

When the impurity ions were  $\text{Mg}^{2+}$ ,  $\text{Cr}^{x+}$  and  $\text{Mn}^{x+}$ , the conductivity transitions of the doped samples were somewhat different than that of pure BSCF, especially at higher temperatures. The largest effect of the impurity ions was the change in the critical temperature for the transition from semiconducting behavior to metallic conducting behavior in BSCF. Such transition of conductivity behavior is not influenced by the experimental error and is correlated with the nature of the sample itself. So, the slight change in conductivity behavior can reveal the effect of impurity ions in BSCF matrix.

The onset temperature (transition temperature) for transitioning from a metallic conductor to a semiconductor at intermediate temperatures was considerably lower for BSCF containing  $\text{Mn}^{x+}$  than for the other samples. This result can be attributed to the easy reduction of  $\text{Co}^{3+}$  to  $\text{Co}^{2+}$ , as demonstrated by the  $\text{O}_2$ -TPD result. A similar but weak influence can also be observed for BSCF containing a  $\text{Cr}^{x+}$  impurity ion, which may be because the further reduction of  $\text{Co}^{3+}$  in BSCF–Cr1100 was not as enhanced as that in BSCF–Mn1100. For BSCF containing the  $\text{Mg}^{2+}$  impurity, the conductivity tended to decrease as the temperature increased from

~500 to 900 °C, i.e., metallic behavior. This behavior may be caused by two factors: firstly, Mg in the lattice with the stable divalent state and small electronegativity likely blocked the small polar hopping; secondly, the reduced amount of cobalt in B-site could also weaken the hole mobility.

### 3.1.4. Sintering behavior

Generally, slight cation nonstoichiometry and oxygen vacancies can facilitate or inhibit ion mobility [43,44], while the impurity phase(s) in a sample may act as a sintering aid [45] or a grain growth inhibitor [46]. All of these factors affect the sintering behavior of a sample. To investigate the influence of impurity ions on the sintering behavior of BSCF, the surface SEM images of various BSCF membranes with different impurities after sintering are shown in Fig. 6 and the relative densities of the membranes are listed in Table 2. Compared to the pure BSCF membrane, no obvious morphological changes were observed in the various samples, except those containing  $Mg^{2+}$  or  $Cl^-$  impurities. The grain size (2–6  $\mu m$ ) of the BSCF sample containing the  $Mg^{2+}$  impurity was considerably smaller than that of the normal one (9–26  $\mu m$ ), and some small bright particles, which differed from environmental contaminants, were precipitated from the parent phase. The composition of the small particles was examined with EDS, and they were found to be rich in Mg and Co. Together with the XRD results, it was determined that these precipitated particles were mainly composed of CoO. In addition, the relative density of the Mg-containing BSCF membrane was 88.3%, which is higher than that of the pure BSCF membrane. Gong et al. observed that doping a small amount of  $Mg^{2+}$  into the B-site of LSCF could suppress grain growth and enhance the sintering ability of LSCF [47]. In this study, it appears that Mg produced a similar effect on BSCF. In addition, the precipitated CoO, a common sintering aid, could also facilitate sintering of the membrane. In contrast, the sample containing the  $Cl^-$  impurity exhibited poor sintering ability. The grains in the membrane were not well connected, and a markedly low relative density of 77.6% was obtained. This loose microstructure explains the poor mechanical strength of the sample and may be due to the continuous volatilization

of chlorine during sintering at high temperatures. The relative densities of the membranes containing the  $Na^+$  and  $K^+$  impurities were slightly lower than that of the pure membrane. It appears that the presence of additional  $Na^+$  or  $K^+$  in the A-site of BSCF prevented its sintering. A similar phenomenon was also observed in the A-site cation-enriched BSCF and can be attributed to diffusion of the restrained A-site cation during the sintering process. Interestingly, it appears that the sintering ability of BSCF was not influenced by presence of  $Ca^{2+}$  in its lattice. With an excess of  $Cr^{x+}$  and  $Mn^{x+}$  in the B-site, a higher relative density was observed. This result could be attributed to the improved mobility of the A-site cation, which facilitated the sintering of BSCF. Moreover, the sintering capability of BSCF doped with  $Cr^{x+}$  was even better. The distinct large lattice parameters along with the large free space likely further enhanced the mobility of ions during calcination. Silica is generally used as a high-temperature sintering aid; however, the sintering ability of BSCF containing the silicon impurity was not improved and a relatively low density of 86.0% was obtained. This result can be explained by the presence of silica with a high melting point did not effectively function as a sintering aid at a relatively low calcination temperature [48]; instead, the silica impurity phase(s) may hinder the sintering of BSCF.

## 3.2. Performance

### 3.2.1. Oxygen permeation properties

The oxygen permeation fluxes of the samples are shown in Fig. 7. Similar to the conductivity test, the oxygen permeation flux of the sample containing the  $Cl^-$  impurity cannot be obtained.

**Table 2**

Relative densities of the membranes after calcining at 1100 °C for 5 h.

Impurity ion	Nil <sup>a</sup>	Na <sup>+</sup>	K <sup>+</sup>	Mg <sup>2+</sup>	Ca <sup>2+</sup>	Cr <sup>x+</sup>	Mn <sup>x+</sup>	Si <sup>4+</sup>	Cl <sup>-</sup>
Relative density (%)	87.2	86.7	86.6	88.3	87.4	88.6	88	86	77.6

<sup>a</sup> Nil represents the BSCF membrane with no impurity ions.

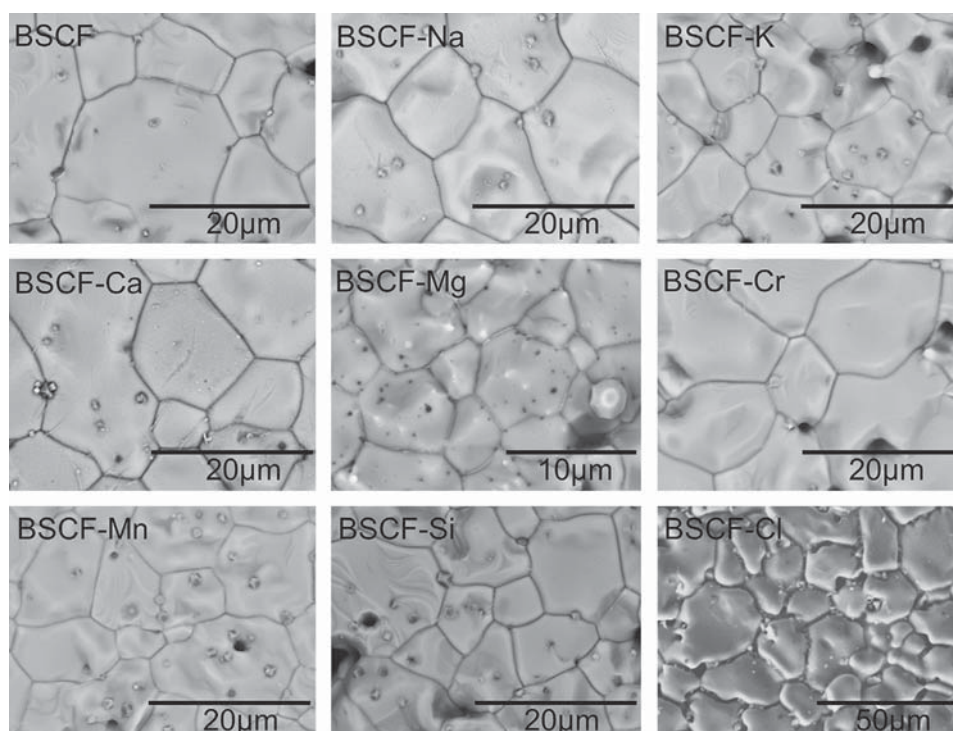


**Fig. 6.** Surface SEM images of the various BSCF membranes with different impurities.

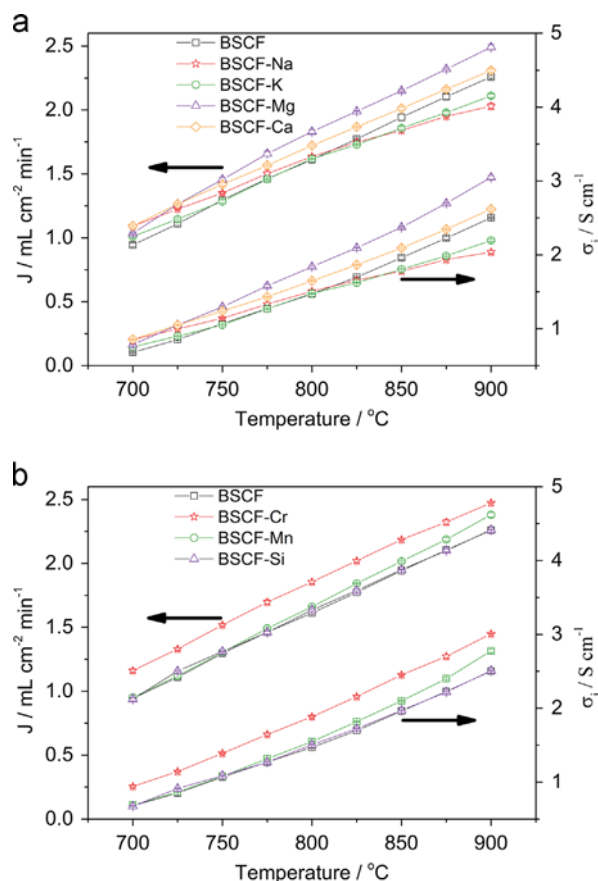


**Fig. 7.** Temperature dependence of the oxygen permeation fluxes and oxygen ionic conductivities of various BSCF samples.

Notably, the samples with  $\text{Na}^+$ ,  $\text{K}^+$  and  $\text{Ca}^{2+}$  impurities exhibited similar oxygen permeation trends, i.e., the oxygen permeation flux decreased slower than for pure BSCF. As an example, the oxygen permeation flux of BSCF-K1100 was slightly lower than that of BSCF at 900 °C, but it was higher than that of BSCF at 700 °C. It appears that both Mg and Cr had a positive effect on the oxygen permeation of BSCF, whereas the positive effect of Mn was not obvious. The slight silica impurity seemingly had little impact on the oxygen permeation flux of the BSCF membrane.

If the oxygen permeation flux is controlled by the bulk oxygen diffusion, the oxygen permeation flux of the membrane can be expressed with Wagner's equation,

$$J_{\text{O}_2} = -\frac{RT}{4^2 F^2 L} \int_{\ln P_{\text{O}_2}}^{\ln P'_{\text{O}_2}} \frac{\sigma_e \sigma_i}{\sigma_e + \sigma_i} d(\ln P_{\text{O}_2})$$

here  $L$  is the thickness of the membrane,  $\sigma_e$  is the electronic conductivity,  $\sigma_i$  is the oxygen ionic conductivity, while  $P'_{\text{O}_2}$  and  $P_{\text{O}_2}$  are the oxygen partial pressure at oxygen-rich side and oxygen-lean side of the membrane, respectively.

The ionic conductivity of the membrane is a key factor that influences the performance of oxygen permeation membrane. As discussed above, the electrical conductivity of BSCF containing impurity ions did not change a lot. So it can be considered that the electronic conductivities of BSCF doped with impurity ions should be sufficiently higher than their ionic conductivities. Then the ionic conductivity can be calculated according to the oxygen permeation flux with the equation as follow:

$$\sigma_i = J_{\text{O}_2} \times \frac{4^2 F^2 L}{RT} \times \left( \ln \frac{P'_{\text{O}_2}}{P_{\text{O}_2}} \right)^{-1}$$

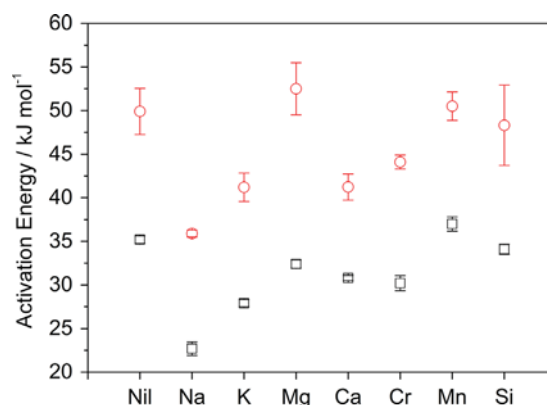


**Fig. 8.** Calculated apparent activation energy of various BSCF membranes in the high temperature region (black squares) and low temperature region (red circles). (For interpretation of the references to color in this figure legend, the reader is referred to the web version of this article.)

From the equation, it can be found that the ionic conductivity is approximately proportional to the oxygen permeation flux. The calculated ionic conductivities are exhibited in Fig. 7. Indeed, the trend of the ionic conductivity is similar to that of the corresponding oxygen permeation flux. So the influence of impurity ions on the ionic conductivity of BSCF can be plausibly correlated to the variation of the oxygen permeation flux of the BSCF caused by impurity ions.

To further analyze the impact of impurity ions on the oxygen permeation flux of the BSCF membranes, Arrhenius plots of the oxygen permeation flux of the samples were drawn. It was found that the temperature dependence of the oxygen permeation flux over the entire temperature range (from 700 to 900 °C) cannot be described as single Arrhenius behavior. With the temperature of 800 °C as the transition point, the flux can be roughly divided into two parts according to the Arrhenius behavior. This division can be explained by the fact that the oxygen permeation of the BSCF membrane was rate-determined by both a bulk diffusion process and surface oxygen exchange kinetics, and as the temperature decreased, the surface oxygen exchange kinetics with a higher activation energy (compared with the bulk diffusion process) contributed more to the apparent activation energy of BSCF. The calculated apparent activation energy is shown in Fig. 8. For all samples, the apparent activation energy of the high temperature region was much lower than the corresponding activation energy of the low temperature region. This trend revealed that the small amount of impurity ions in BSCF did not have a strong impact on the oxygen permeation mechanism of BSCF. It was also observed that the membranes containing Na, K, and Ca impurities had lower apparent activation energies in both temperature regions. The reduced activation energy may be due to the improved surface oxygen exchange kinetics, and a similar result was also observed in the slightly B-site deficient BSCF membrane [15]. Further study is needed to study such obviously reduced activation energy. The activation energy of BSCF containing the  $\text{Mg}^{2+}$  impurity in the low temperature region was higher than that of pure BSCF, whereas the activation energy in the high temperature region was lower. This result reveals that with the presence of the  $\text{Mg}^{2+}$  impurity, the bulk diffusion of oxygen became easier, which consequently improved the oxygen permeation flux. As demonstrated previously, the grain size of BSCF containing the Mg impurity was much smaller than that of pristine BSCF; it has been reported that the oxygen permeation performance of BSCF was inversely proportional to the grain size [49]. Hence, the enhanced bulk oxygen diffusion was likely due to the improved relative density of the membrane. Similarly, the better sintering of the  $\text{Cr}^{x+}$ -doped BSCF

membrane can explain its reduced activation energy and its improved oxygen permeation flux. For  $Mn^{x+}$  and  $Si^{4+}$  as impurity ions, the changes in the activation energy and oxygen permeation flux of the BSCF membrane were not as pronounced compared to the membrane with  $Cr^{x+}$  and  $Mg^{2+}$  as impurity ions. This result suggests that both  $Mn^{x+}$  in the crystal lattice and silica at the grain boundary and in the phase reaction product(s) had negligible effects on the oxygen permeability of the BSCF membranes.

### 3.2.2. Activity for oxygen reduction

Electrochemical impedance spectra (EIS) were obtained from the samples to evaluate the effects of the impurity ions on the electrochemical activity of BSCF for oxygen reduction. Because most of the impurity ions were doped into the BSCF lattice during the preparation of the electrodes (1000 °C for 2 h), it is reasonable to hypothesize that the effects of the various impurity ions on BSCF are similar between the sample calcined at 1000 °C and the sample calcined at 1100 °C. Fig. 9 presents the EIS of the various BSCF electrodes containing impurity ions measured using the symmetrical cell configuration at 650 °C. It can be observed that the EIS of the electrode with pure BSCF and those with BSCF containing Na, Si and Cl impurities are similar, with two observable arcs representing two different oxygen reduction processes, whereas the EIS of the remainder of the samples show one additional arc. To further clarify

the effects of impurities on the oxygen reduction activity of BSCF, two equivalent circuits of L-Rohm-(R1-CPE1)-(R2-CPE2) and L-Rohm-(R1-CPE1)-(R1'-CPE1')-(R2-CPE2), as shown in Fig. 9, were used to fit the EIS data of those containing two arcs and three arcs, respectively. The L and Rohm in the equations represent the inductance and the ohmic resistance from the testing system, respectively. A combination of parallel R (resistor) and CPE (constant phase element) represents one electrode process. The EIS can be well fitted with the above equivalent circuits, and the results from fitting the EIS data at 650 °C are shown in Table 3. Generally, the impedance arc with an angular relaxation frequency ( $f$ ) at approximately 10–1000 Hz and a capacitance ( $C$ ) at approximately  $0.01$ – $0.1 \text{ F cm}^{-2}$  can be attributed to a charge transfer process, and the arc representing a surface diffusion process has a lower frequency and a larger capacitance [50]. Based on the fitting results, it can be deduced that the arcs fitted with (R1-CPE1) and (R1'-CPE1') at high frequency can be attributed to a charge transfer process, whereas the arc fitted with (R2-CPE2) at low frequency can be attributed to a surface diffusion process.

The fitting electrode resistances and the activation energy for the oxygen reduction processes on different BSCF electrodes are listed in Table 4. As shown in the table, the charge transfer resistance ( $Re1$ ) increased while the surface diffusion resistance ( $Re2$ ) reduced slightly when  $Na^+$  and  $K^+$  were introduced as more oxygen vacancies were formed, facilitating oxygen adsorption and

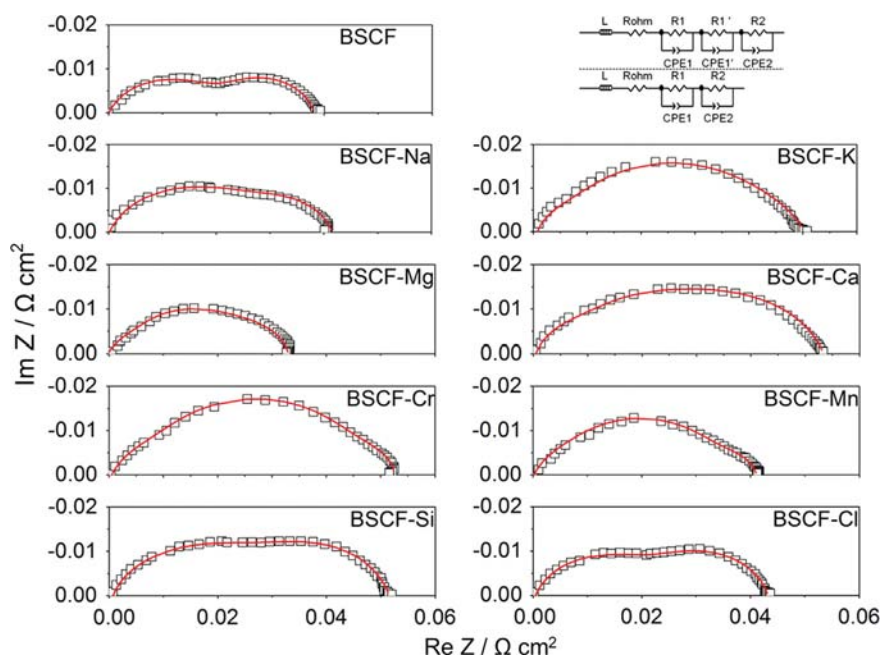


Fig. 9. Equivalent circuits applied for fitting and the fitted EIS of symmetrical cells at 650 °C with various impurity ions doped into BSCF used as electrodes.

Table 3

The results from fitting the EIS data of various BSCF electrodes containing different impurity ions at 650 °C.

Impurity ion	Nil <sup>a</sup>	Na <sup>+</sup>	K <sup>+</sup>	Mg <sup>2+</sup>	Ca <sup>2+</sup>	Cr <sup>x+</sup>	Mn <sup>x+</sup>	Si <sup>4+</sup>	Cl <sup>-</sup>
R1 ( $\Omega \text{ cm}^2$ )	0.0272	0.0351	0.00862	0.00748	0.0108	0.0112	0.00928	0.0360	0.0270
C1 ( $\text{F cm}^{-2}$ )	0.00767	0.0103	0.0203	0.0144	0.0160	0.0105	0.0130	0.0120	0.00762
f1 (Hz)	762.1	440.8	911.5	1481	915.7	1340	1340	381.6	800.7
R1' ( $\Omega \text{ cm}^2$ )	–	–	0.0338	0.0186	0.0210	0.0383	0.0279	–	–
C1' ( $\text{F cm}^{-2}$ )	–	–	0.0910	0.0886	0.107	0.0857	0.0751	–	–
f1' (Hz)	–	–	51.77	96.80	71.21	48.36	76.82	–	–
R2 ( $\Omega \text{ cm}^2$ )	0.0158	0.0104	0.00910	0.0107	0.0226	0.00606	0.00729	0.0182	0.0195
C2 ( $\text{F cm}^{-2}$ )	3.565	2.831	5.382	1.547	0.7831	10.76	8.634	1.405	1.012
f2 (Hz)	2.833	5.411	3.007	9.654	8.991	2.435	2.557	6.415	8.312

<sup>a</sup> Nil represents the BSCF electrode with no impurity ions.

**Table 4**  
Fitting electrode resistances and the activation energies ( $E_a$ ) for Rp of different BSCF electrodes.

Impurity ion	650 °C			600 °C			550 °C			500 °C			$E_a$ /kJ mol <sup>-1</sup>
	Re1 <sup>a</sup>	Re2	Rp	Re1	Re2	Rp	Re1	Re2	Rp	Re1	Re2	Rp	
Nil	0.0272	0.0158	0.0430	0.0510	0.0458	0.0967	0.098	0.200	0.298	0.196	0.978	1.173	131.6 ± 5.6
Na <sup>+</sup>	0.0351	0.0104	0.0455	0.0608	0.0348	0.0936	0.120	0.145	0.266	0.234	0.764	0.998	122.8 ± 6.8
K <sup>+</sup>	0.0424	0.0091	0.0515	0.0977	0.0294	0.123	0.214	0.138	0.353	0.463	0.763	1.22	125.1 ± 2.6
Mg <sup>2+</sup>	0.0260	0.0107	0.0367	0.0573	0.0323	0.0896	0.115	0.150	0.2657	0.264	0.760	1.024	131.8 ± 3.6
Ca <sup>2+</sup>	0.0318	0.0226	0.0544	0.0701	0.052	0.128	0.164	0.216	0.381	0.346	1.07	1.41	129.3 ± 3.7
Cr <sup>x+</sup>	0.0495	0.0060	0.0555	0.0996	0.0224	0.121	0.203	0.116	0.320	0.475	0.601	1.076	117.3 ± 3.6
Mn <sup>x+</sup>	0.0371	0.0073	0.0444	0.071	0.019	0.091	0.153	0.0914	0.245	0.361	0.411	0.772	113.7 ± 3.9
Si <sup>4+</sup>	0.0360	0.0182	0.054	0.0721	0.0635	0.136	0.151	0.281	0.432	0.295	1.402	1.697	136.8 ± 3.3
Cl <sup>-</sup>	0.0270	0.0195	0.046	0.0565	0.0527	0.109	0.102	0.242	0.345	0.213	1.39	1.611	140.4 ± 7.6

<sup>a</sup> Re1 = R1 + R1' for BSCF electrodes containing K<sup>+</sup>, Mg<sup>2+</sup>, Ca<sup>2+</sup>, Cr<sup>x+</sup> and Mn<sup>x+</sup> impurity ions.

diffusion. In contrast, for the sample with Ca<sup>2+</sup> as an impurity ion, both Re1 and Re2 increased. This result may be correlated with the decreased lattice parameters and the weak reduction activity of Co/Fe in BSCF containing the Ca<sup>2+</sup> impurity. For the BSCF with the Mg<sup>2+</sup> impurity, the electrode resistance Rp decreased. In the temperature range for electrode testing, the precipitated CoO can be oxidized to Co<sub>3</sub>O<sub>4</sub>, which can improve the electrode performance of BSCF. Therefore, the reduced electrode resistance can be attributed to the synergistic effect of Co<sub>3</sub>O<sub>4</sub> [51]. Additionally, it appears that the (Ba, Sr)CoO<sub>3</sub> phase, which is also a product from the BSCF phase transition [52], had no detrimental impact on the performance of BSCF. A similar observation was also reported by Chen et al. [26]. The BSCF electrodes with Cr<sup>x+</sup> and Mn<sup>x+</sup> impurities showed much lower activation energies of 117.3 and 113.7 kJ mol<sup>-1</sup>, respectively. Due to the reduced surface diffusion resistance, the electrode performance was improved as the temperature decreased, especially for the electrode containing the Mn<sup>x+</sup> impurity, although their charge transfer resistance was slightly higher than that of pure BSCF. We have previously demonstrated that doping Cr<sup>x+</sup> into BSCF substantially expanded the crystal lattice and that doping Mn<sup>x+</sup> into BSCF strongly influenced the flexibility in changing the valence states of Co/Fe, both of which could promote surface oxygen diffusion. The detrimental effect of silica in BSCF was notable, as both the charge transfer and surface diffusion resistances increased. Therefore, both amorphous silica and the phase reaction products would hinder the oxygen reaction activity of BSCF. The Cl<sup>-</sup> in BSCF did not influence its charge transfer process, but the surface diffusion process was impacted according to the increased Re2. Overall, although small changes in the electrode activation energy and in the oxygen reduction process were observed, the effects of impurities on the activity of BSCF for oxygen reduction are only modest, especially at temperatures of 600 °C and higher.

#### 4. Conclusions

In the present work, the impacts of small amounts of impurity ions in BSCF on its properties and performance for use as CMs for oxygen separation or as electrodes for oxygen reduction were systematically investigated. With the exception of the BSCF samples containing Mg<sup>2+</sup> and Si<sup>4+</sup> impurities, the BSCF samples doped with other impurity ions did not exhibit a phase transition or form an impurity phase. The influence of impurity ions on the electrical conductivity of BSCF was not obvious. Doping Mg<sup>2+</sup> into the BSCF lattice reduced the grain size of BSCF, whereas doping Cl<sup>-</sup> into the BSCF lattice hindered the sintering of BSCF and consequently resulted in the poor mechanical strength of the CM. The change in the oxygen permeation flux of the CMs can be explained by both the different sintering abilities of BSCF CMs caused by the different impurity ions

and the different sites the impurity ions occupied. The oxygen reduction process on the BSCF electrode was slightly influenced by the presence of various impurity ions, and it was correlated with the site where the impurity ions were doped or the formation of impurity phase(s). In summary, except chloride, the presence of impurity ions in BSCF at relatively high level has less impact on the performance of BSCF for use as CMs for oxygen separation and as electrodes for oxygen reduction. Despite the case that several impurity ions co-exist in BSCF is not studied here, it can be expected that the influence should be a combined effects. The overall effects include the impacts when the impurity ions are doped into BSCF separately and should be mild. Therefore, the BSCF material can be synthesized using low purity raw materials to reduce the preparation costs, which increase the competitiveness of BSCF in the fields of CMs and SOFCs.

#### Acknowledgments

This work was supported by the “National Science Foundation for Distinguished Young Scholars of China” under Contract no. 51025209 and Dr. Zongping Shao acknowledges the ARC future fellowship.

#### References

- [1] B.C.H. Steele, J.M. Bae, Properties of La<sub>0.6</sub>Sr<sub>0.4</sub>Co<sub>0.2</sub>Fe<sub>0.8</sub>O<sub>3-x</sub> (LSCF) double layer cathodes on gadolinium-doped cerium oxide (CGO) electrolytes II. Role of oxygen exchange and diffusion, *Solid State Ionics* 106 (1998) 255–261.
- [2] S. Wang, T. Chen, S. Chen, Kinetics of oxygen reduction over Sm<sub>0.5</sub>Sr<sub>0.5</sub>CoO<sub>3</sub> supported on La<sub>0.9</sub>Sr<sub>0.1</sub>Ga<sub>0.8</sub>Mg<sub>0.2</sub>O<sub>3</sub>, *J. Electrochem. Soc.* 151 (2004) A1461–A1467.
- [3] L. Wang, R. Merkle, J. Maier, Surface kinetics and mechanism of oxygen incorporation into Ba<sub>1-x</sub>Sr<sub>x</sub>Co<sub>0.7</sub>Fe<sub>0.3</sub>O<sub>3-δ</sub> SOFC Microelectrodes, *J. Electrochem. Soc.* 157 (2010) B1802–B1808.
- [4] K. Watanabe, M. Yuasa, T. Kida, Y. Teraoka, N. Yamazoe, K. Shimano, High-performance oxygen-permeable membranes with an asymmetric structure using Ba<sub>0.95</sub>La<sub>0.05</sub>FeO<sub>3-δ</sub> perovskite-type oxide, *Adv. Mater.* 22 (2010) 2367–2370.
- [5] F. Dong, D. Chen, Y. Chen, Q. Zhao, Z. Shao, La-doped BaFeO<sub>3-δ</sub> perovskite as a cobalt-free oxygen reduction electrode for solid oxide fuel cells with oxygen-ion conducting electrolyte, *J. Mater. Chem.* 22 (2012) 15071–15079.
- [6] Z. Liu, L. Cheng, M. Han, A-site deficient Ba<sub>1-x</sub>Co<sub>0.7</sub>Fe<sub>0.2</sub>Ni<sub>0.1</sub>O<sub>3-δ</sub> cathode for intermediate temperature SOFC, *J. Power Sources* 196 (2011) 868–871.
- [7] W. Zhou, R. Ran, Z. Shao, Progress in understanding and development of Ba<sub>0.5</sub>Sr<sub>0.5</sub>Co<sub>0.8</sub>Fe<sub>0.2</sub>O<sub>3-δ</sub>-based cathodes for intermediate-temperature solid-oxide fuel cells: a review, *J. Power Sources* 192 (2009) 231–246.
- [8] Z. Shao, W. Yang, Y. Cong, H. Dong, J. Tong, G. Xiong, Investigation of the permeation behavior and stability of a Ba<sub>0.5</sub>Sr<sub>0.5</sub>Co<sub>0.8</sub>Fe<sub>0.2</sub>O<sub>3-δ</sub> oxygen membrane, *J. Membr. Sci.* 172 (2000) 177–188.
- [9] Z. Shao, S.M. Haile, A high-performance cathode for the next generation of solid-oxide fuel cells, *Nature* 431 (2004) 170–173.
- [10] S. Li, Z. Lv, N. Ai, K. Chen, W. Su, Electrochemical performance of (Ba<sub>0.5</sub>Sr<sub>0.5</sub>)<sub>0.9</sub>Sm<sub>0.1</sub>Co<sub>0.8</sub>Fe<sub>0.2</sub>O<sub>3-δ</sub> as an intermediate temperature solid oxide fuel cell cathode, *J. Power Sources* 165 (2007) 97–101.
- [11] H. Lu, J. Tong, Z. Deng, Y. Cong, W. Yang, Crystal structure, oxygen permeability and stability of Ba<sub>0.5</sub>Sr<sub>0.5</sub>Co<sub>0.8</sub>Fe<sub>0.1</sub>M<sub>0.1</sub>O<sub>3-δ</sub> (M = Fe, Cr, Mn, Zr) oxygen-permeable membranes, *Mater. Res. Bull.* 41 (2006) 683–689.

- [12] L. Bi, E. Fabbri, E. Traversa, Novel  $\text{Ba}_{0.5}\text{Sr}_{0.5}(\text{Co}_{0.8}\text{Fe}_{0.2})_{1-x}\text{Ti}_x\text{O}_{3-\delta}$  ( $x=0, 0.05$ , and  $0.1$ ) cathode materials for proton-conducting solid oxide fuel cells, *Solid State Ionics* 214 (2012) 1–5.
- [13] S.M. Fang, C.Y. Yoo, H.J.M. Bouwmeester, Performance and stability of niobium-substituted  $\text{Ba}_{0.5}\text{Sr}_{0.5}\text{Co}_{0.8}\text{Fe}_{0.2}\text{O}_{3-\delta}$  membranes, *Solid State Ionics* 195 (2011) 1–6.
- [14] L. Ge, W. Zhou, R. Ran, S. Liu, Z. Shao, W. Jin, N. Xu, Properties and performance of A-site deficient ( $\text{Ba}_{0.5}\text{Sr}_{0.5}$ ) $_{1-x}\text{Co}_{0.8}\text{Fe}_{0.2}\text{O}_{3-\delta}$  for oxygen permeating membrane, *J. Membr. Sci.* 306 (2007) 318–328.
- [15] L. Ge, R. Ran, K. Zhang, S. Liu, Z. Shao, Oxygen selective membranes based on B-site cation-deficient ( $\text{Ba}_{0.5}\text{Sr}_{0.5}$ )( $\text{Co}_{0.8}\text{Fe}_{0.2}$ ) $_y\text{O}_{3-\delta}$  perovskite with improved operational stability, *J. Membr. Sci.* 318 (2008) 182–190.
- [16] W. Zhou, R. Ran, Z. Shao, W. Zhuang, J. Jia, H. Gu, W. Jin, N. Xu, Barium- and strontium-enriched ( $\text{Ba}_{0.5}\text{Sr}_{0.5}$ ) $_{1+x}\text{Co}_{0.8}\text{Fe}_{0.2}\text{O}_{3-\delta}$  oxides as high-performance cathodes for intermediate-temperature solid-oxide fuel cells, *Acta Mater.* 56 (2008) 2687–2698.
- [17] W. Zhou, R. Ran, Z. Shao, W. Jin, N. Xu, Evaluation of A-site cation-deficient ( $\text{Ba}_{0.5}\text{Sr}_{0.5}$ ) $_{1-x}\text{Co}_{0.8}\text{Fe}_{0.2}\text{O}_{3-\delta}$  ( $x > 0$ ) perovskite as a solid-oxide fuel cell cathode, *J. Power Sources* 182 (2008) 24–31.
- [18] S. Li, Z. Lv, X. Huang, W. Su, Thermal, electrical, and electrochemical properties of Nd-doped  $\text{Ba}_{0.5}\text{Sr}_{0.5}\text{Co}_{0.8}\text{Fe}_{0.2}\text{O}_{3-\delta}$  as a cathode material for SOFC, *Solid State Ionics* 178 (2008) 1853–1858.
- [19] J.M. Porras-Vazquez, P.R. Slater, Synthesis of oxyanion-doped barium strontium cobalt ferrites: stabilization of the cubic perovskite and enhancement in conductivity, *J. Power Sources* 209 (2012) 180–183.
- [20] A. Sadhu, T. Kramer, A. Datta, S.A. Wiedigen, J. Norpoth, C. Jooss, S. Bhattacharyya, Ferromagnetism in lightly doped  $\text{Pr}_{1-x}\text{Ca}_x\text{MnO}_3$  ( $x=0.023, 0.036$ ) nanoparticles synthesized by microwave irradiation, *Chem. Mater.* 24 (2012) 3758–3764.
- [21] B. Raveau, A. Maignan, C. Martin, Insulator–metal transition induced by Cr and Co doping in  $\text{Pr}_{0.5}\text{Ca}_{0.5}\text{MnO}_3$ , *J. Solid State Chem* 130 (1997) 162–166.
- [22] M.D. Glinchuk, I.P. Bykov, S.M. Kornienko, V.V. Laguta, A.M. Slipenyuk, A.G. Bilous, O.I. Vyunov, O.Z. Yanchevskii, Influence of impurities on the properties of rare-earth-doped barium–titanate ceramics, *J. Mater. Chem.* 10 (2000) 941–947.
- [23] E. Bucher, C. Gspan, F. Hofer, W. Sitte, Sulphur poisoning of the SOFC cathode material  $\text{La}_{0.6}\text{Sr}_{0.4}\text{CoO}_{3-\delta}$ , *Solid State Ionics* 238 (2013) 15–23.
- [24] M.M. Viitanen, R.G.V. Welzenis, H.H. Brongersma, F.P.F. Berkel, Silica poisoning of oxygen membranes, *Solid State Ionics* 150 (2002) 223–228.
- [25] Y.M. Kim, X.B. Chen, S.P. Jiang, J. Bae, Chromium deposition and poisoning at  $\text{Ba}_{0.5}\text{Sr}_{0.5}\text{Co}_{0.8}\text{Fe}_{0.2}\text{O}_{3-\delta}$  cathode of solid oxide fuel cells, *Electrochem. Solid-State Lett.* 14 (2011) B41–B45.
- [26] Y. Chen, F. Wang, D. Chen, F. Dong, H.J. Park, C. Kwak, Z. Shao, Role of silver current collector on the operational stability of selected cobalt-containing oxide electrodes for oxygen reduction reaction, *J. Power Sources* 210 (2012) 146–153.
- [27] B.H. Toby, A graphical user interface for GSAS, *J. Appl. Crystallogr.* 34 (2001) 210–213.
- [28] P. Thompson, D.E. Cox, J.B. Hastings, Rietveld refinement of Debye–Scherrer synchrotron X-ray data from  $\text{Al}_2\text{O}_3$ , *J. Appl. Crystallogr.* 20 (1987) 79–83.
- [29] A.D. Handoko, G.K.L. Goh, Hydrothermal synthesis of sodium potassium niobate solid solutions at 200 °C, *Green Chem.* 12 (2010) 680–687.
- [30] S. Hou, J.A. Alonso, J.B. Goodenough, Co-Free, iron perovskites as cathode materials for intermediate-temperature solid oxide fuel cells, *J. Power Sources* 195 (2010) 280–284.
- [31] V.V. Kharton, A.P. Viskup, A.V. Kovalevsky, F.M. Figueiredo, J.R. Jurado, A.A. Yaremchenko, E.N. Naumovich, J.R. Frade, Surface-limited ionic transport in perovskites  $\text{Sr}_{0.97}(\text{Ti}, \text{Fe}, \text{Mg})\text{O}_{3-\delta}$ , *J. Mater. Chem.* 10 (2000) 1161–1169.
- [32] J.M. Porras-Vazquez, E.R. Losilla, P.J. Keenan, C.A. Hancock, T.F. Kemp, J.V. Hanna, P.R. Slater, Investigation into the effect of Si doping on the performance of  $\text{Sr}_{1-y}\text{Ca}_y\text{MnO}_{3-\delta}$  SOFC cathode materials, *Dalton Trans.* 42 (2013) 5421–5429.
- [33] H.X. Dai, C.F. Ng, C.T. Au, Perovskite-type halo-oxide  $\text{La}_{1-x}\text{Sr}_x\text{FeO}_{3-\delta}\text{X}_x$  ( $\text{X}=\text{F}, \text{Cl}$ ) catalysts selective for the oxidation of ethane to ethene, *J. Catal.* 189 (2000) 52–62.
- [34] R.D. Shannon, Revised effective ionic radii and systematic studies of interatomic distances in halides and chalcogenides, *Acta Crystallogr. A* 32 (1976) 751–767.
- [35] X. Liu, W. Su, Z. Lu, J. Liu, L. Pei, W. Liu, L. He, Mixed valence state and electrical conductivity of  $\text{La}_{1-x}\text{Sr}_x\text{CrO}_3$ , *J. Alloys Compd.* 305 (2000) 21–23.
- [36] M. Arnold, Q. Xu, F.D. Tichelaar, A. Feldhoff, Local charge disproportion in a high-performance perovskite, *Chem. Mater.* 21 (2009) 635–640.
- [37] H.X. Dai, C.F. Ng, C.T. Au,  $\text{YBa}_2\text{Cu}_3\text{O}_{7-\delta}\text{X}_x$  ( $\text{X}=\text{F}$  and  $\text{Cl}$ ): highly active and durable catalysts for the selective oxidation of ethane to ethene, *J. Catal.* 193 (2000) 65–79.
- [38] J.F. Liu, S. Yin, H.P. Wu, Y.W. Zeng, X.R. Hu, Y.W. Wang, G.L. Lv, J.Z. Jiang, Wurtzite-to-rocksalt structural transformation in nanocrystalline  $\text{CoO}$ , *J. Phys. Chem. B* 110 (2006) 21588–21592.
- [39] Y. Yao, J. Zhang, L. Xue, T. Huang, A. Yu, Carbon-coated  $\text{SiO}_2$  nanoparticles as anode material for lithium ion batteries, *J. Power Sources* 196 (2011) 10240–10243.
- [40] C. Zener, Interaction between the d-shells in the transition metals. II. Ferromagnetic compounds of manganese with perovskite structure., *Phys. Rev.* 82 (1951) 403–405.
- [41] A.S. Harvey, Z. Yang, A. Infortuna, D. Beckel, J.A. Purton, L.J. Gauckler, Development of electron holes across the temperature-induced semiconductor–metal transition in  $\text{Ba}_{1-x}\text{Sr}_x\text{Co}_{1-y}\text{Fe}_y\text{O}_{3-\delta}$  ( $x, y=0.2-0.8$ ): a soft X-ray absorption spectroscopy study, *J. Phys. Condens. Matter.* 21 (2009) 015801.
- [42] A.S. Harvey, F.J. Litterst, Z. Yang, J.L.M. Rupp, A. Infortuna, L.J. Gauckler, Oxidation states of Co and Fe in  $\text{Ba}_{1-x}\text{Sr}_x\text{Co}_{1-y}\text{Fe}_y\text{O}_{3-\delta}$  ( $x, y=0.2-0.8$ ) and oxygen desorption in the temperature range 300–1273 K, *Phys. Chem. Chem. Phys.* 11 (2009) 3090–3098.
- [43] J.W. Stevenson, P.F. Hallman, T.R. Armstrong, L.A. Chick, Sintering behavior of doped lanthanum and yttrium manganite, *J. Am. Ceram. Soc.* 78 (1995) 507–512.
- [44] R.D. Levi, Y. Tsur, The effect of oxygen vacancies in the early stages of  $\text{BaTiO}_3$  nanopowder sintering, *Adv. Mater.* 17 (2005) 1606–1608.
- [45] V.V. Kharton, A.L. Shaula, F.M.M. Snijkers, J.F.C. Coymans, J.J. Luyten, I. P. Marozau, A.P. Viskup, F.M.B. Marques, J.R. Frade, Oxygen transport in ferrite-based ceramic membranes: effects of alumina sintering aid, *J. Eur. Ceram. Soc.* 26 (2006) 3695–3704.
- [46] Y. Chen, D. Chen, R. Ran, H.J. Park, C. Kwak, S.J. Ahn, K.S. Moon, Z. Shao, A New Way to increase performance of oxide electrode for oxygen reduction using grain growth inhibitor, *Electrochem. Commun.* 14 (2012) 36–38.
- [47] Z. Gong, X. Yin, L. Hong, Modification of B-site doping of perovskite  $\text{La}_x\text{Sr}_{1-x}\text{Fe}_{1-y-z}\text{Co}_y\text{Cr}_z\text{O}_{3-\delta}$  oxide by  $\text{Mg}^{2+}$  ion, *Solid State Ionics* 180 (2009) 1471–1477.
- [48] C. Salle, A. Maitre, J. Baumard, Y. Rabinovitch, A first approach of silica effect on the sintering of Nd: YAG, *Opt. Rev.* 14 (2007) 169–172.
- [49] H. Wang, C. Tablet, A. Feldhoff, J. Caro, Investigation of phase structure, sintering, and permeability of perovskite-type  $\text{Ba}_{0.5}\text{Sr}_{0.5}\text{Co}_{0.8}\text{Fe}_{0.2}\text{O}_{3-\delta}$  membranes, *J. Membr. Sci.* 262 (2005) 20–26.
- [50] M.J. Escudero, A. Aguadero, J.A. Alonso, L. Daza, A kinetic study of oxygen reduction reaction on  $\text{La}_2\text{NiO}_4$  cathodes by means of impedance spectroscopy, *J. Electroanal. Chem.* 611 (2007) 107–116.
- [51] D. Chen, C. Huang, R. Ran, H.J. Park, C. Kwak, Z. Shao, New  $\text{Ba}_{0.5}\text{Sr}_{0.5}\text{Co}_{0.8}\text{Fe}_{0.2}\text{O}_{3-\delta}+\text{Co}_3\text{O}_4$  composite electrode for IT-SOFCs with improved electrical conductivity and catalytic activity, *Electrochem. Commun.* 13 (2011) 197–199.
- [52] K. Efimov, Q. Xu, A. Feldhoff, Transmission electron microscopy study of  $\text{Ba}_{0.5}\text{Sr}_{0.5}\text{Co}_{0.8}\text{Fe}_{0.2}\text{O}_{3-\delta}$  perovskite decomposition at intermediate temperatures, *Chem. Mater.* 22 (2010) 5866–5875.